Available online at www.sciencedirect.com
SCIENCE DIRECT
Journal of Photochemistry and Photobiology A: Chemistry 177 (2006) 116–124
Journal of Photochemistry and Photobiology A:Chemistry
www.elsevier.com/locate/jphotochem

Photolysis of glyoxal in air☆

Jovan Tadić [a], Geert K. Moortgat [b,*], Klaus Wirtz [c]

[a] *Faculty of Chemistry, University of Belgrade, P.O. Box 158, 11001 Belgrade, Serbia and Montenegro*
[b] *Max-Planck-Institut Für Chemie, Atmospheric Chemistry Department, P.O. Box 3060, 55020 Mainz, Germany*
[c] *Fundación CEAM, Parque Technologico, 46980 Paterna, Valencia, Spain*

Available online 17 November 2005

Dedicated to Professor R.P. Wayne.

Abstract

The photolysis of glyoxal in synthetic air was investigated in a quartz cell at 298 K using three types of UV sources (TL/12 lamps (275–380 nm), TL/03 lamps (390–470 nm) and mercury lamps (254 nm)) and products were identified and quantitatively analyzed using long-path FTIR spectroscopy. For all light sources, the observed products were CO, HCHO and HCOOH. Absolute quantum yields were determined using Cl_2 and Br_2 as actinometers. Photolysis in the first absorption band of glyoxal, using TL/12 lamps, provided an overall quantum yield of $\Phi_T = 0.97 \pm 0.05$, independent of total pressure ranging from 100 to 700 Torr air. The absolute quantum yields obtained with the TL/03 lamps, covering the second absorption band of glyoxal, showed dependency on total pressure, ranging from $\Phi_T = 0.12$ at 100 Torr to $\Phi_T = 0.042$ at 700 Torr, which can be expressed as a Stern–Volmer-type equation $1/\Phi_T = (6.80 + 251.8) \times 10^{-4} \times P$ (Torr).

By combining the product yields with literature data, we deduced the detailed picture of glyoxal photolysis, including the dependency of the quantum yield of each particular channel: CHOCHO + $h\nu \rightarrow$ 2HCO (Φ_1); CHOCHO + $h\nu \rightarrow H_2 + 2CO$ (Φ_2); CHOCHO + $h\nu \rightarrow H_2CO + CO$ (Φ_3) on the applied wavelength. The product quantum yields indicate that dissociation into two HCO radicals is the most important pathway under atmospheric conditions. The mean photolysis rate was measured under solar radiation in the EUPHORE outdoor chamber to be $J_{obs} = 1.04 \pm 0.10 \times 10^{-4}\ s^{-1}$, corresponding to a mean effective quantum yield $\phi_{eff} = 0.035 \pm 0.007$. Although glyoxal has a very low effective quantum yield, photolysis remains an important removal path in the atmosphere.

Keywords: Glyoxal; Photolysis; Quantum yields; Photodissociation rates

1. Introduction

Glyoxal, HCOCHO, the simplest α-dicarbonyl, is an atmospheric relevant carbonyl compound and is formed as product in the photooxidation of simple volatile organic compounds (VOC) in air in the presence of NO_x. In particular, glyoxal has been observed as an important ring-cleavage product in the OH-initiated oxidation of aromatic hydrocarbons in air, in the presence of NO_x [1–4]. For example, in a recent study performed in the outdoor simulation chamber, the primary yield of glyoxal was found to be $35 \pm 10\%$ for benzene and about 5% higher for toluene and *p*-xylene. These glyoxal yields are considerably larger than those established in most of the previous photooxidation studies [5 and references cited therein].

Glyoxal was also identified as a product of the reaction of O_3 and/or OH radicals with alkenes [6,7] and unsaturated oxygen-containing VOC, such as acrolein [8], also in the OH-initiated oxidation of acetylene [9,10] and glycolaldehyde [11]. Glyoxal has been observed in car exhaust emissions [12,13]. A few measurements of glyoxal in the urban environment atmosphere have been reported [14–16] with mixing ratios ranging from 100 ppt to a few ppb.

The most important removal process in the atmosphere during daytime is photolysis, with minor contributions coming form the reaction with OH radicals [17]. The atmospheric residence time with respect to photolysis has been reported to be a few hours [17,18].

☆ This paper was mistakenly omitted from the special issue of *Journal of Photochemistry and Photobiology, A: Chemistry* (volume 176, issues 1–3, 14 December 2005), which is dedicated to the honour of Professor R.P. Wayne. The Publisher apologises for any inconvenience caused.

* Corresponding author.
E-mail address: moo@mpch-mainz.mpg.de (G.K. Moortgat).

1010-6030/$ – see front matter © 2005 Elsevier B.V. All rights reserved.
doi:10.1016/j.jphotochem.2005.10.010

Glyoxal exhibits an absorption spectrum consisting of two main absorption bands: a broad UV band between 220 and 350 nm and a stronger structured band in the range 350–480 nm. Brand [19] recognized that the latter band consists of two band systems, an extremely weak one with its 0–0 band at 520.8 nm and another relatively much stronger one with its 0–0 band at 454.9 nm. The absorption cross-sections have been reported in several studies [17,20–22]. The sharp peak at 455 nm has been used to measure glyoxal with the differential optical absorption spectroscopy (DOAS) technique in an outdoor simulation chamber [5] and in urban air [16].

Theoretically, the photolysis of glyoxal can occur through the following channels:

$$\mathrm{CHOCHO} + h\nu \rightarrow 2\mathrm{HCO};$$
$$\Delta H^{\circ}_{298} = 68.5\,\mathrm{kcal/mol}; \quad \lambda_{\mathrm{threshold}} \leq 417\,\mathrm{nm} \qquad (1)$$

$$\mathrm{CHOCHO} + h\nu \rightarrow \mathrm{H_2} + 2\mathrm{CO};$$
$$\Delta H^{\circ}_{298} = -2.1\,\mathrm{kcal/mol}; \quad \mathrm{all}\,\lambda \qquad (2)$$

$$\mathrm{CHOCHO} + h\nu \rightarrow \mathrm{H_2CO} + \mathrm{CO};$$
$$\Delta H^{\circ}_{298} = -1.7\,\mathrm{kcal/mol}; \quad \mathrm{all}\,\lambda \qquad (3)$$

$$\mathrm{CHOCHO} + h\nu \rightarrow \mathrm{H} + \mathrm{CO} + \mathrm{HCO};$$
$$\Delta H^{\circ}_{298} = 85.4\,\mathrm{kcal/mol}; \quad \lambda_{\mathrm{threshold}} \leq 334\,\mathrm{nm} \qquad (4)$$

Calvert and Pitts [23] summarized the quantum yield data before 1966 and are presented in Table 1a. Based on the work of Calvert and Layne [24], it was established that channel (3) was the dominant photolysis channel (yield 0.84–0.6 in the range 254–435 nm) with little evidence for the radical channel (1). At 313 nm, Plum et al. [17] measured a quantum yield for HCHO of 0.13 for wavelengths larger than 325 nm, but reported an "effective quantum yield" of $\phi_{\mathrm{eff}} = 0.029$, based on measured outdoor relative photolysis rates compared to NO_2, $J_{\mathrm{CHOCHO}}/J_{\mathrm{NO_2}} = 0.008 \pm 0.005$. Langford and Moore [25] determined HCO directly by resonance absorption and deduced total HCO yields of 0.8 ± 0.4 ($\Phi_1 \approx 0.4$) at 305 nm and estimated quantum yield for the other two channels. Using cavity ring-down spectroscopy, Zhu et al. [26] found HCO yields of 1.5 ($\Phi_1 \approx 0.75$) at 351 nm, 0.69 ($\Phi_1 \approx 0.35$) at 308 nm, 0.52 ($\Phi_1 \approx 0.26$) at 248 nm and 0.42 ($\Phi_1 \approx 0.21$) at 193 nm. Those quantum yield data are summarized in Table 1b. Obviously, the reliable high quantum yields reported by Zhu et al. [26] at 351 nm ($\Phi_1 \approx 0.75$) are in conflict with the earlier yields reported by Calvert for $\Phi_3 = 0.6$ at 366 nm.

Table 1a
Photolysis of glyoxal as given in Calvert and Pitts [23]

CHOCHO + hν	<253.7 nm	253.7 nm	313 nm	366 nm	435 nm
→2HCO (Φ_1)	≠0		0	0	
→H_2 + 2CO (Φ_2)		0.16	0.15	0.02	0.01
→HCHO + CO (Φ_3)		0.84	0.85	0.7	0.6

Table 1b
Photolysis of CHOCHO, yields of Zhu et al. [26] and Langford and Moore [25]

CHOCHO + hν	Zhu et al.				Langford and Moore
	193 nm	248 nm	308 nm	351 nm	308 nm
→2HCO (Φ_1)	0.21	0.26	0.35	0.75	0.4
→H_2 + 2CO (Φ_2)					0.15
→HCHO + CO (Φ_3)					0.45

Table 1c
Photolysis of CHOCHO, quantum yields of HCO radical, from Chen and Zhu [27]

λ (nm)	$\Phi^{\circ}_{\mathrm{HCO}}$	λ (nm)	$\Phi^{\circ}_{\mathrm{HCO}}$	Φ_{HCO} at 760 Torr N_2
290	0.50 ± 0.01	360	1.62 ± 0.15	
300	0.68 ± 0.02	370	1.49 ± 0.04	
310	0.84 ± 0.07	380	1.91 ± 0.13	0.49
320	1.43 ± 0.02	390	2.01 ± 0.08	0.54
330	1.77 ± 0.12	400	0.74 ± 0.08	0.32
340	1.54 ± 0.01	410	0.56 ± 0.04	0.22
350	1.34 ± 0.06	420	0.48 ± 0.03	0.14

More recently, Chen and Zhu [27] used cavity ring-down spectroscopy and reported the dependence of the HCO quantum yield in the wavelength range 290 to 420 nm on the glyoxal (1–8 Torr) pressure and nitrogen buffer gas (10–400 Torr). For pure glyoxal photolysis, these authors reported zero pressure HCO quantum yields ($\Phi^{\circ}_{\mathrm{HCO}}$) at 10 nm intervals, to increase from 0.50 ± 0.01 at 290 nm to a maximum of 2.01 ± 0.08 at 390 nm and to drop to 0.74 ± 0.08 at 400 nm, 0.56 ± 0.04 at 410 nm and 0.48 ± 0.03 at 420 nm. HCO quantum yield were found independent of N_2-gas in the 290–370 nm region, but decreased with increasing pressure in the 380–420 nm region. They deduced HCO quantum yields at 760 Torr N_2 to be 0.49 at 380 nm, 0.54 at 390 nm, 0.32 at 400 nm, 0.22 at 410 nm and 0.14 at 420 nm. The reported HCO quantum yields are summarized in Table 1c.

According to the results of Zhu et al. [26] and Chen and Zhu [27] the photolysis of glyoxal in the atmosphere is an important source of HCO radicals, which are readily converted into HO_2 radicals and thus affect other photochemical transformation processes [1]. The investigation of the quantum yields of glyoxal photolysis is necessary to estimate its atmospheric fate and role.

Products analysis and quantum yields were determined by photolysing dilute mixtures of glyoxal in air using three types of light sources (TL12 lamps (Philips, 40 W), TL03 lamps (Philips, 40 W) and mercury lamps) photolysing both main absorption bands with broad-band emission lamps. These investigations showed that the total quantum yield of CHOCHO removal of the photolysis within the first absorption band (220–350 nm) is close to unity, while photolysis within the second band (350–470 nm) band shows strong pressure dependency, indicating absolute quantum yields much lower than 1. The yields of the different channels can be, at least partially, deduced from the product yields of the glyoxal decomposition in both absorption bands obtained in this work and available literature data.

2. Experimental

2.1. Experiments performed in Mainz

The photooxidation experiments were carried out in a long-path quartz cell with detection of products by FTIR spectroscopy. After identification and quantification of the products, a mechanistic description of the photooxidation was deduced. From the measured decay rate of starting glyoxal concentration, overall quantum yields for photolysis were calculated comparing with the decay rate of a selected actinometer.

The apparatus employed in this work have been described elsewhere [8,28,29] and will only be discussed here briefly. The central part of the apparatus is a 44.2 l quartz cell equipped with two independent sets of White-optics mirror arrangements. Sapphire-coated aluminium mirrors were used for IR measurements, while MgF_2-coated aluminium mirrors were used for UV–visible absorption measurements. The base distance between the mirrors was 1.2 m. The IR and UV path lengths were tuned to 28 passes (33.6 m) and 8 passes (9.82 m), respectively. In the infrared region the photolysis educts and products were measured, while in the UV–visible region the photolysis rates of the actinometers Cl_2 and Br_2 were determined. Infrared spectra at 0.5 cm^{-1} resolution (450–4000 cm^{-1}) were measured with a Bomem DA3-FTIR spectrometer. This method provides the possibility of simultaneous detection and monitoring of all IR-active products and the starting material.

Experiments were carried out at room temperature (298 K), at total pressures between 100 and 700 Torr (1 Torr = {101,325/760} Pa), with initial mixing ratios 40–320 ppm. Photolysis was achieved with six radially mounted lamps, TL/12-sunlamps (Philips 40 W), TL/03 lamps (40 W) or mercury lamps (strongest emission at 254 nm) all in different experiments. The TL/12 fluorescent lamps emit in the region 275–380 nm, with a maximum at 310 nm, whereas the TL/03 lamps emit in the region 390–470 nm, with a maximum at 425 nm. Fig. 1 displays the emission spectra of the lamps combined with the absorption spectrum. Spectra were taken every 5–10 min with a total irradiation time varying between 30 and 60 min. Qualitative and quantitative data evaluation were carried out by comparing the products spectra with reference spectra obtained in the same cell and using calibration curves at corresponding pressures and resolution [28–30].

The use of a continuous broad-band light source allows only the determination of an integral, effective quantum yield Φ^{int} for the photoactive region. Quantum yields (absolute) were calculated according to the following equation (for carbonyl compound C and actinometer Act) (I):

$$\Phi^{int}(C) = \frac{K_{Phot}(C)}{(K_{Phot}(Act))(\sum OV(C))/\sum OV(Act) \times \Phi^{int}(Act)} \quad (I)$$

Chlorine and bromine were used as actinometers, both with $\Phi = 1$, in experiments with TL/12 and TL/03 lamps, respectively [31]. The quantum yield is the only unknown parameter in Eq. (I): the photolysis rates K_{phot} for both compound and actinometers can be directly measured and the terms $\sum$OV(C) and $\sum$OV(Act) represent the calculated overlap of proper lamp and absorption spectra.

2.2. Experiments performed at EUPHORE

A detailed description of the EUPHORE facility and the existing analytical equipment can be found in references [11,32]. It consists of two 200 m^3 independent hemispherical outdoor simulation chambers, made of FEP foil (more than 80% transmis-

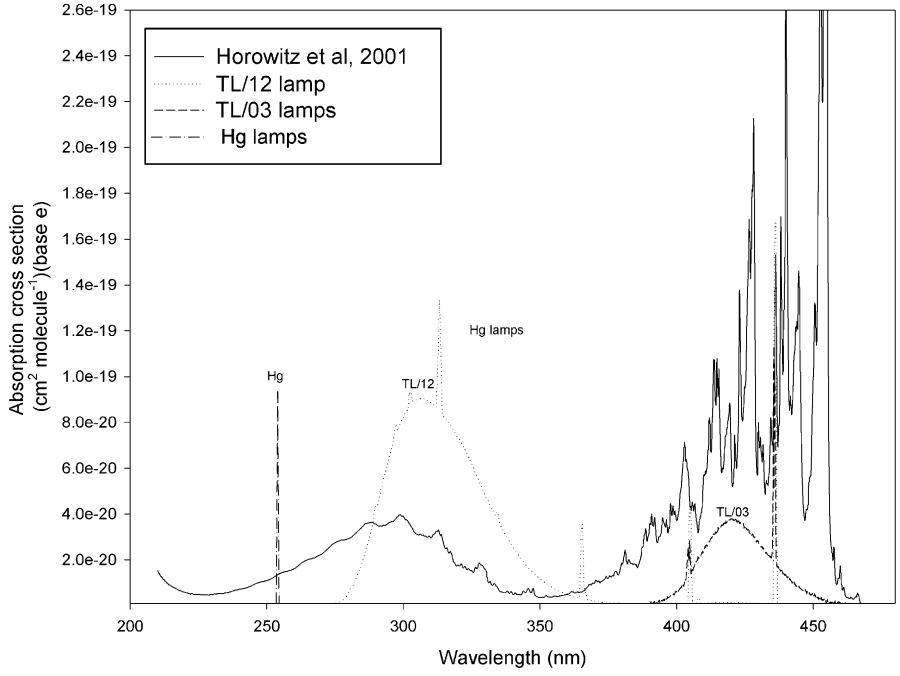

Fig. 1. Absorption cross-section of glyoxal, after Horowitz et al. [21] and emission spectra of the Hg, TL/12 and TL/03 lamps, given in arbitrary units.

sion of the solar radiation in the wavelength range 290–520 nm). Both chambers are equipped with FTIR spectrometers coupled with White-type multi-path mirror systems for in situ analysis (optical path lengths of 326.8 and 553.5 m). The IR spectra were recorded every 10 min by co-adding 550 interferograms with a resolution of 1 cm^{-1}. Gas chromatographs equipped with different detectors, such as FID, PID and ECD were also used for analysis. Reactant and product concentrations were determined using calibrated reference spectra.

Known amounts of glyoxal were introduced into the chambers in the concentration range 0.34–0.74 ppm along with SF_6, which was used as a tracer in the determinations of the dilution rate caused by minor leaks by thermal expansion of the reaction mixture and by the sampling for analysis. In some experiments, cyclohexane or di-*n*-butyl ether (DNBE) was added to scavenge OH radicals or to estimate their concentration. OH radicals are formed because trace amounts of NO_x, i.e. ($NO + NO_2$) are present in the chamber. The stability of the reaction mixtures prior to their exposure to sunlight, i.e. the possibility of dark reactions was examined by starting the analytical sampling at least 30 min before the onset of photolysis. The presence of an excess of cyclohexane ($[cyclohexane]_0/[glyoxal]_0 > 20$ minimizes the consumption of glyoxal due to a reaction with OH and the OH chemistry of the observed products. On the other hand, the use of the tracer, DNBE, enables estimation of the OH concentration in the chamber during the photolysis experiments. The OH concentration is derived from the first order decay of the tracer concentration and it is then used to estimate the contribution of the OH reaction to the loss of glyoxal.

3. Materials

Glyoxal trimeric dihydrate (≥99.2%) was obtained from Aldrich Chemical Co. Pure glyoxal was produced by heating glyoxal trimeric dihydrate in the presence of P_2O_5 (sicapent) to 150 °C and condensing the glyoxal vapor in a separate vessel cooled with dry ice/ethanol mixture [25]. Glyoxal was collected as yellow crystals and was stored at dark place, at temperature about −20 °C. The purity was checked by FTIR spectroscopy, which is also used for monitoring the photooxidation process. Di-*n*-butyl ether (>99%) was obtained from Fluka, cyclohexane (≥99.9%) and Br_2 (>99.5%) from Aldrich and Cl_2 (>99.8%) and C_2H_6 (99.95%) from Linde.

4. Results and discussion

4.1. Products

As products of photolysis, CO (2037–2235 cm^{-1}), HCHO (2895–2898 cm^{-1}) and HC(O)OH (1105 cm^{-1}) were detected using all three types of UV sources and calibrated reference spectra are available for these compounds [28–30]. Glyoxal was monitored using the specific absorption peaks at 1740 and/or 2847 cm^{-1}. Measured absorption coefficients for glyoxal are $(3.56 \pm 0.29) \times 10^{-19}$ cm^2 $molecule^{-1}$ (base 10) at 1740 cm^{-1} and $(1.33 \pm 0.10) \times 10^{-19}$ cm^2 $molecule^{-1}$ at 2847 cm^{-1}. Integrated absorption cross-sections

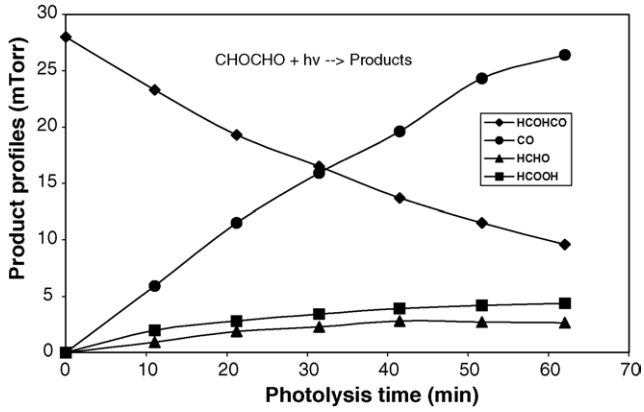

Fig. 2. Typical time profiles of the partial pressures of glyoxal, CO, HCHO and HC(O)OH during photolysis using TL/12 lamps.

are $(1.03 \pm 0.10) \times 10^{-17}$ cm^2 $molecule^{-1}$ for the range 1643–1807 cm^{-1} and $(7.21 \pm 0.56) \times 10^{-18}$ cm^2 $molecule^{-1}$ for the range 2737–2921 cm^{-1}.

The appearance of HC(O)OH can be explained as secondary product of the reaction initiated by the reaction of HO_2 radicals with HCHO [33–36]:

$$HCHO + HO_2 \rightarrow HOCH_2O_2$$
$$\rightarrow \cdots \rightarrow HC(O)OH, CH_3OH, HO_2$$

Since the only precursor of HC(O)OH is HCHO, the sum of the quantities of both compounds was used for the determination of the importance of the channel leading to the formation of HCHO.

Typical time profiles of partial pressures of glyoxal, CO, HCHO and HC(O)OH, during the photolysis with TL/12 lamps, are shown in Fig. 2. The time profiles of the partial pressures using other sources of irradiation are similar in shape, but with difference in the quantities CO and HCHO formed. Their ratio is proven to be dependent on the photolysis wavelength, which corresponds to the different decomposition channels.

Before we discuss the impact that our measurements have on the understanding of the glyoxal photodecomposition channels, the occurrence of the photolysis channel (4) must be considered. Reaction (4) is thermodynamically allowed and was mentioned in recent work of Zhu et al. [26] and Chen and Zhu [27]. The latter authors measured only the HCO radical yield and obtained a maximum zero pressure quantum yield $\Phi^{\circ}_{HCO} = 2.01 \pm 0.08$ at 390 nm, which was uniquely attributed to channel (1). In order to explain the lower HCO radical yields at higher photolysing energies, they invoked the simultaneous occurrence of photolysis channels (1) and (4) in the range 320–370 nm, although the calculated photochemical threshold for process (4) is 334 nm. No other photolysis channels were considered to explain the decreasing quantum yields at $\lambda < 390$ nm.

Process (4) would be a cleavage process of two independent bonds without forming a cyclic transition state and thus can hardly be viewed as a strictly single photon process or even less probably a concerted one. The non-consideration of this photolysis channel is important for the calculation of absolute quantum yields of the three channels (1)–(3), fully describing

Table 2
The probability of the sum of channels (1) + (2) and (3) channel, for all three sources of UV radiation (error limits represent experimental scatter)

Mercury lamps		TL/12 lamps		TL/03 lamps	
Channels[a] (1) + (2)	Channel[b] (3)	Channels (1) + (2)	Channel[b] (3)	Channels (1) + (2)	Channel[b] (3)
0.68	0.32	0.74	0.26	0.88	0.12
0.69	0.31	0.76	0.24	0.84	0.16
0.71	0.29	0.75	0.25	–	–
0.67	0.33	0.69	0.31	0.86	0.14
0.62	0.38	0.71	0.29	0.79	0.21
0.66	0.34	0.73	0.27	–	–
0.67	0.33	0.71	0.29	0.86	0.14
0.71	0.29	0.71	0.29	0.83	0.17
0.64	0.36	0.72	0.28	–	–
–	–	0.72	0.28	0.84	0.16
0.66	0.34	0.74	0.26	0.85	0.15
–	–	0.69	0.31	–	–
0.66 ± 0.05	0.34 ± 0.05	0.72 ± 0.04	0.28 ± 0.04	0.84 ± 0.05	0.16 ± 0.05

[a] The yield of channels (1) + (2) is given by the yield of CO–[HCHO + HC(O)OH].
[b] The yield of channel (3) is given by the yield of [HCHO + HC(O)OH].

the primary step of glyoxal photolysis under our experimental conditions. Moreover, the yield of CO measured in this study cannot be distinguished to arise from channels (1) or (4). Similarly, the following thermodynamically allowed process will not be considered:

$$CHOCHO + h\nu \rightarrow H + H + 2CO \quad (5)$$

The consideration of channel (1) itself is essential, since HCO radicals have directly been measured by Zhu et al. [26] and Chen and Zhu [27]. Under our applied conditions in synthetic air, all formed HCO radicals quantitatively react with oxygen, giving CO and HO_2 [1]:

$$HCO + O_2 \rightarrow CO + HO_2 \quad (6)$$

causing the inability of distinguishing channels (1) and (2) and consequently must be considered only as the sum in the subsequent analysis.

The probability for the glyoxal molecule to undergo decomposition channels (1) + (2) and (3) using different UV sources, can be deduced from the products CO and HCHO + HC(O)OH as is presented in Table 2. The yield of channel (3) is represented by the yield of HCHO + HC(O)OH, whereas the yield of channels (1) + (2) is given by the yield of CO–[HCHO + HC(O)OH]. Results using TL/12 and TL/03 represent only mean values in the specified wavelength ranges.

4.2. Absolute quantum yield

One of the objectives of the study was to determine the absolute quantum yield dependency on total pressure, in the various regions of the photolysis lamps. As is mentioned above, to achieve this goal experiments were done with proper actinometers: chlorine was used for the TL/12, while bromine for TL/03 lamps. Ethane was used in both cases as Cl- and Br-atom scavenger. From the decay of glyoxal, the photolytic rates were deduced for the different pressures by plotting the natural logarithm of concentration versus time (first-order decay) and performing a regression analysis. From these results, overall quantum yields were calculated according to Eq. (I) using the overlap integrals of glyoxal/TL/12 or glyoxal/TL/03 and Cl_2/TL/12 or Br_2/TL/03 and the experimentally determined photolysis rates of both actinometers using proper lamps.

In the case of TL/12 lamps, absolute quantum yields have been determined to be 0.97 ± 0.05, independent of total pressures ranging from 100 to 700 Torr, as is seen in Table 3. It has been assumed to be also unity in the case of mercury lamps.

On the contrary, the absolute quantum yields for the region covered by the TL/03 lamps (at $\lambda > 390$ nm), decrease from near 0.12 at 100 Torr to 0.0425 at 700 Torr, thus showing a significant variation with pressure. These values are shown in Table 4. This pressure dependence can be represented by a Stern–Volmer plot, as is shown in Fig. 3, where $1/\Phi_T$ is plotted versus total pressure.

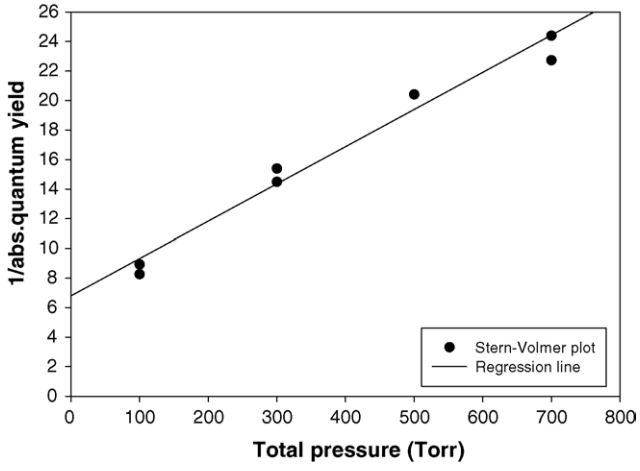

Fig. 3. Stern–Volmer plot of glyoxal ($1/\Phi_T$ vs. P) irradiated at room temperature with TL/03 lamps.

Table 3
Absolute quantum yields in the photolysis of glyoxal using TL/12 lamps, measured at different total pressures

Total pressure (Torr)	Initial glyoxal (mTorr)	$K_{phot} \times 10^3$ (min^{-1})	Absolute quantum yield	Average quantum yield
100	32.41	15.54	0.915	
100	28.54	15.79	0.930	
100	28.88	17.04	1.004	0.950 ± 0.048
300	31.87	15.43	0.909	
300	27.87	16.25	0.957	
300	24.51	17.10	1.007	0.958 ± 0.049
500	30.87	15.33	0.907	
500	32.28	16.44	0.968	
500	28.38	17.37	1.023	0.966 ± 0.058
700	30.02	17.73	1.044	
700	30.63	16.08	0.947	
700	33.54	17.61	1.037	1.009 ± 0.054
				Average = 0.971 ± 0.051

A fit through the data gives Eq. (II):

$$\frac{1}{\Phi_T} = 6.80 + 251.8 \times 10^{-4} \times P\,(\text{Torr}). \quad \text{(II)}$$

The zero pressure overall quantum yield ($\Phi_{T,0} = 0.147$) is much lower than unity indicating that other energy dissipating processes play a significant role [37–39].

These results, along with the determination of the relative product yields and in combination with previously published data, provide sufficient information for the construction of the picture of wavelength dependence of the quantum yields of glyoxal at atmospheric pressure. The total quantum yield in Fig. 4 is presented with a solid line and was constructed in analogy to the wavelength dependency of the total quantum yield in the photolysis of methylglyoxal photolysis by Koch and Moortgat [40], that has a very similar absorption spectrum as glyoxal. At atmospheric pressure, the total quantum yield decreases rapidly at the wavelength, where the second absorption band begins near 350 nm. Indeed, the total quantum yield Φ_T in the TL/03 range (390–470 nm) is 0.0425 ± 0.002, as seen in Table 4.

In order to establish the course of the yield of the radical channel (Φ_1), the data obtained by the data of Zhu et al. [26] and Chen and Zhu [27] are used. The Φ°_{HCO} values listed in Table 1c reflect the total HCO radicals produced via channel (1), therefore, the contribution of channel (1) is $\Phi_1 = 0.5\Phi^{\circ}_{HCO}$. It is to be noted that these authors did not observe a total pressure dependence (using N_2) of the HCO radical yield for glyoxal photolysis below 380 nm. However, a pronounced pressure dependence of the Φ_{HCO} was observed in the range 380–420 nm, from which $\Phi^{760\,Torr}_{HCO}$ was deduced, as shown in the right column of Table 1c.

Table 4
Absolute quantum yields in the photolysis of glyoxal using TL/03 lamps measured at different total pressures

Total pressure (Torr)	Absolute quantum yield	Average absolute quantum yields
100	0.112	
100	0.121	0.117 ± 0.005
300	0.069	
300	0.065	0.067 ± 0.002
500	0.049	
500	0.049	0.049
700	0.044	
700	0.041	0.0425 ± 0.002

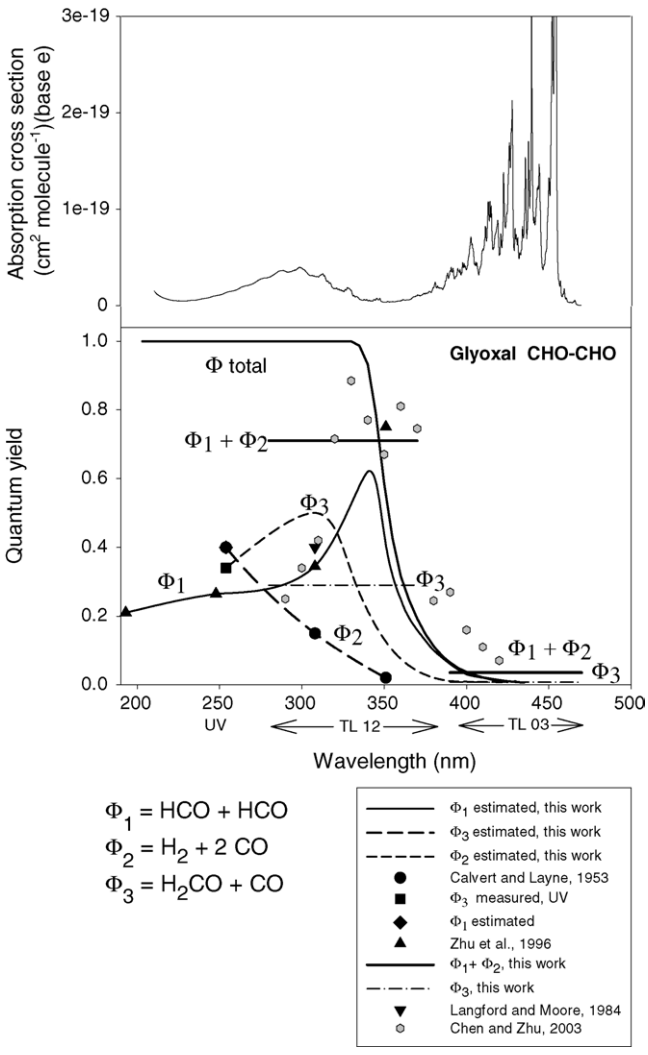

Fig. 4. Total quantum yield and channel yields dependency on the wavelength at 700 Torr.

The yield of the radical channel Φ_1 as determined by Zhu et al. [26] increases from 0.21 at 193 nm to reach a maximum near 0.75 ± 0.08 at 350 nm. The quantum yield for the radical channel (1) of Chen and Zhu [27] clusters in the range 320–370 nm near a value 0.77 ± 0.08 (see Table 1c). As mentioned above, at longer wavelengths 390–470 nm (in the range of the TL/03 lamps), our data show much lower quantum yields ($\Phi_T = 0.0425$ at 700 Torr). Therefore, the course of Φ_1 will have a local maximum near 350 nm and will then decrease with increasing wavelength, as shown in Fig. 4. Also, the data of Chen and Zhu [27] demonstrate a sharp drop of Φ_1 to near 0.25 at 380–390 nm, further decreasing to 0.07 at 420 nm.

According to Table 2, the *relative* yield of the sum of channels (1) + (2) = 0.84 ± 0.05 for the TL/03 lamps, the absolute contribution of ($\Phi_1 + \Phi_2$) being, therefore, 0.036 ± 0.002 at 700 Torr and $\Phi_3 = 0.007 \pm 0.002$. For the TL/12 lamps (270–380 nm), the total yield $\Phi_T = (\Phi_1 + \Phi_2 + \Phi_3)$ is assumed to be unity (exactly 0.97 ± 0.05), independent of pressure and using the data of Table 2, the quantum yields are ($\Phi_1 + \Phi_2$) = 0.72 ± 0.04 and $\Phi_3 = 0.28 \pm 0.04$. Our measurements at 254 nm also provide information for ($\Phi_1 + \Phi_2$) = 0.66 ± 0.05 and $\Phi_3 = 0.34 \pm 0.05$. At this wavelength assuming $\Phi_T = 1$ and using $\Phi_1 = 0.26$ from Zhu et al. [26], Φ_2 is estimated to be $\Phi_2 = 0.40 \pm 0.04$. The wavelength dependence of the Φ_2 curve can thus be assessed combining this value with the data of Calvert and Layne [24], at 313 and 366 nm to be 0.15 and 0.02, respectively, as seen in Fig. 4.

The quantum yield curve for channel (3) over the region 254–350 nm can be constructed from the value $\Phi_3 = 0.45$ estimated by Langford and Moore [25] at 308 nm and our measurements with the Hg-lamp at 254 nm ($\Phi_3 = 0.34 \pm 0.05$) and the TL/12 lamps ($\Phi_3 = 0.28 \pm 0.04$). At longer wavelengths, Φ_3 must decrease steadily to reach the value of 0.007 in the range 390–470 nm, as obtained by the TL/03 lamps.

The course of the quantum yield curves of the three channels is represented in Fig. 4 and the quantum yields are listed in Table 5. At wavelengths shorter than 335 nm, the total quantum yield Φ_T is unity and starts to drop sharply at longer wavelengths to reach zero near 450 nm. It has to be noted that the overlap of the TL/12 lamps (270–380 nm) with the first absorption band (225–350 nm) is not complete in the long wavelength range near 350 nm, as seen in Fig. 1. At the start of the drop of Φ_T at 335 nm, the TL/12 lamps still emit a significant portion (ca. 15%) of their light. The experimental quantum yield 0.97 ± 0.05 in the emission range of the TL/12 lamps might, therefore, be fortuitous, but maybe even too high. The quantum yields were calculated using the absorption cross-sections from Horowitz et al. [21]. During the course of this work, new glyoxal absorption cross-sections have been reported by Volkamer et al. [22], which were on average 5–8% larger than the values measured by Horowitz et al. [21]. Assuming these higher absorption coefficients might solve this apparent discrepancy.

The course of the Φ_1 curve at wavelengths longer than 350 nm is largely determined by the quantum yield values ($\Phi_1 + \Phi_2$) = 0.036 ± 0.002 at 700 Torr obtained by the TL/03 lamps in the range 390–470 nm. Assuming that $\Phi_2 = 0$ at $\lambda > 360$ nm (see Fig. 4) and that the thermodynamic threshold for process (1) is 417 nm [27], the average yield for Φ_1 becomes 0.036 in the range 390–417 nm. This average value for Φ_1 is much smaller than the values deduced by Chen and Zhu [27] for Φ_1 from the $0.5\Phi_{HCO}^{760\,Torr}$ yield, dropping from 0.27 at 390 nm to 0.07 at 420 nm. The proposed Φ_1 curve from this work is, therefore, displaced toward shorter wavelengths with regards to the data points reported by Chen and Zhu [27].

The error associated with the reported quantum yields as listed in Table 5 is difficult to assess, since they is based on an interpolation of the product yields of the glyoxal decomposition in both absorption bands obtained in this work and available literature data obtained at selective wavelengths. Although the

Table 5
Absolute quantum yield and channel yields at different wavelength of UV radiation as constructed from literature data and our measurements (see text)

λ (nm)	Φ_{tot}	Φ_1	Φ_2	Φ_3
225	1.0	0.241	0.560	0.199
230	1.0	0.246	0.535	0.219
235	1.0	0.251	0.504	0.245
240	1.0	0.256	0.475	0.269
245	1.0	0.261	0.448	0.291
250	1.0	0.266	0.420	0.314
255	1.0	0.271	0.395	0.334
260	1.0	0.278	0.370	0.352
265	1.0	0.286	0.345	0.369
270	1.0	0.293	0.320	0.387
275	1.0	0.301	0.295	0.404
280	1.0	0.310	0.270	0.420
285	1.0	0.320	0.250	0.430
290	1.0	0.330	0.230	0.440
295	1.0	0.343	0.206	0.451
300	1.0	0.357	0.186	0.457
305	1.0	0.374	0.166	0.460
310	1.0	0.396	0.146	0.458
315	1.0	0.423	0.125	0.452
320	1.0	0.457	0.110	0.433
325	1.0	0.497	0.095	0.408
330	1.0	0.541	0.080	0.379
335	0.995	0.593	0.065	0.337
340	0.978	0.648	0.051	0.279
345	0.856	0.616	0.036	0.204
350	0.691	0.520	0.021	0.150
355	0.540	0.424	0.008	0.108
360	0.404	0.332	0.0	0.072
365	0.293	0.253		0.040
370	0.213	0.191		0.022
375	0.156	0.142		0.014
380	0.115	0.104		0.011
385	0.085	0.077		0.008
390	0.064	0.057		0.007
395	0.048	0.043		0.005
400	0.037	0.033		0.004
405	0.029	0.026		0.003
410	0.022	0.020		0.002
415	0.017	0.016		0.001
420	0.013	0.013		0.0
425	0.010	0.010		
430	0.008	0.008		
435	0.006	0.006		
440	0.003	0.003		
445	0.001	0.001		

Table 6
Summary of glyoxal experiments at EUPHORE

Date	Concentration (ppm)	Solar zenith angle	OH-tracer	Total removal rate (s^{-1})	Dilution rate (s^{-1})	Tracer removal rate (s^{-1})	NO_2 photolysis rate (s^{-1})	CHOCHO photolysis rate (s^{-1})	Φ_{eff}
23.06.98 (B)[a]	0.481	25	Cyclohexane 23.3 ppm	1.06×10^{-4}	1.23×10^{-5}	–	8.65×10^{-3}	9.37×10^{-5}	0.034
24.06.98 (A)	0.556	21	Di-*n*-butyl ether 129 ppb	1.21×10^{-4}	1.37×10^{-5}	2.78×10^{-5}	9.03×10^{-3}	1.02×10^{-4}	0.037
13.10.99 (B)	0.339	67.3	Cyclohexane 15 ppm	7.94×10^{-5}	5.77×10^{-6}	–	4.32×10^{-3}[b]	7.36×10^{-5}	0.030
14.10.99 (B)	0.567	49.8	No tracer	1.24×10^{-4}	9.95×10^{-6}	–	6.75×10^{-3}	1.14×10^{-4}	0.043
15.10.99 (B)	0.734	51.6	No tracer	1.17×10^{-4}	9.90×10^{-6}	–	6.90×10^{-3}	1.07×10^{-4}	0.040
19.10.99 (B)	0.524	52.2	Di-*n*-butyl ether 129 ppb	7.73×10^{-5}	1.36×10^{-5}	1.87×10^{-5}	5.01×10^{-3}	6.18×10^{-5}	0.023
								Average Φ_{eff} =	0.035 ± 0.007

Note: Glyoxal was introduced in different ways during those two campaigns. In June 1998, it was directly introduced by heating and in October 1999, glyoxal was distilled before, from a mixture of glyoxal trimer and sicapent (P_5O_{10}) and then introduced.
[a] Refers to the chamber used.
[b] No radiation after 16:00 h.

experimental scatter of the quantum yield reported in Tables 2–4 are about 5%, systematic errors may include uncertainties in glyoxal (10%) and product concentration (5–10%) and glyoxal absorption cross-sections (10% [21,22]). We, therefore, estimate the overall absolute error in the order of 25–30%.

4.3. EUPHORE experiments

For glyoxal, two experiments have been made in June 1998 and four in October 1999 (for the lower solar conditions). All the photolysis rates are calculated from the decay of glyoxal, measured by FTIR, making the corrections for dilution. Table 6 summarizes the experiments and indicated that photolysis rates range between 6.2×10^{-5} and $11.4 \times 10^{-5}\,s^{-1}$. There is no systematic difference between the experiments performed in June and October. Only, the values in the presence of OH-tracer (October 99) are slightly lower. Thus, the mean photolysis rates for glyoxal J_{CHOCHO} are $(9.78 \pm 0.59) \times 10^{-5}\,s^{-1}$ (in June), $(6.77 \pm 0.83) \times 10^{-5}\,s^{-1}$ (in October with tracer) and $(1.10 \pm 0.05) \times 10^{-4}\,s^{-1}$ (in October without tracer). The observed lower photolysis rates were caused by overcast conditions, reducing the solar intensity and can also be observed in Table 6 from the photolysis rate of NO_2 (J_{NO_2}). An averaged photolysis rate for the cloud-free conditions gives a value of $J_{obs,\,CHOCHO} = 1.04 \pm 0.10 \times 10^{-4}\,s^{-1}$.

The atmospheric photodissociation rate for glyoxal was also calculated by Chen and Zhu [27] using their HCO quantum yield data obtained at 760 Torr total pressure. Assuming a total quantum yield of unity in the range 290–370 nm and $0.5\Phi_{HCO}^{760\,Torr}$ in the range 380–420 nm (these values are listed in Table 1c), their calculations yield J_{diss} in the order of 2.0×10^{-4} to $1.1 \times 10^{-4}\,s^{-1}$ for solar zenith angles (SZA) 0–60°, respectively. These values are up to a factor two larger as observed in the outdoor chamber.

Photolysis frequencies were also calculated by Volkamer et al. using their absorption cross-sections [22] and quantum yields from Ref. [41], which are near identical as in Table 5. They reported $J_{CHOCHO} = 1.15 \times 10^{-4}\,s^{-1}$ for 0° SZA to $5 \times 10^{-5}\,s^{-1}$ at 60° SZA, in good agreement with the values reported in Table 6. Their calculation also showed that more than 80% of the glyoxal photolysis takes place at wavelengths shorter than 370 nm.

It is possible to estimate an average or effective quantum yield Φ_{eff} for glyoxal under typical sunlight conditions. By knowing the absorption spectrum as measured in the laboratory and assuming quantum yield of unity $\Phi_T = (\Phi_1 + \Phi_2 + \Phi_3)$, the photolysis rate was calculated using a simple transfer model [18,38] to be $J_{model} = 2.72 \times 10^{-3}\,s^{-1}$. The effective quantum yield can then be calculated from $\Phi_{eff} = J_{obs}/J_{model} = 0.038$. Effective quantum yields were also determined for each particular photolysis experiment by taking into account the measured local actinic fluxes [41] and are listed calculated in Table 6. An average effective quantum yield was obtained $\Phi_{eff} = 0.035 \pm 0.007$, in agreement with the model calculation.

Finally, this effective quantum yield $\Phi_{eff} = 0.035 \pm 0.007$ is in good agreement with the value reported by Plum et al. [17] $\Phi_{eff} = 0.029$, based on measured outdoor relative photolysis rates compared to NO_2, $k_{CHOCHO}/k_{NO_2} = 0.008 \pm 0.005$. Volkamer et al. [22] also determined $\Phi_{eff} = 0.035 \pm 0.01$ in excellent agreement with the values reported in this study.

5. Atmospheric implications

The atmospheric lifetimes of glyoxal with regard to reaction with OH ($k_{OH} = 1.10 \times 10^{-11}\,cm^3\,molecule^{-1}\,s^{-1}$ [33]) and with regard to "photolysis" are estimated to be $\tau_{OH} = 25$ h (with $[OH] = 10^6$ molecule cm^{-3}), $\tau_{OH} = 5$ h (with $[OH] = 5 \times 10^6$ molecule cm^{-3}) and $\tau_{phot} \approx 3$ h (with 2.8 h if $J_{CHOCHO} = 9.78 \times 10^{-5}\,s^{-1}$, 4.1 h if $J_{CHOCHO} = 6.77 \times 10^{-5}\,s^{-1}$ and finally 2.5 h if $J_{CHOCHO} = 1.10 \times 10^{-4}\,s^{-1}$). Thus, for glyoxal the photolysis is the dominant degradation process, although the effective cross-sections are very low. The product quantum yields indicate that dissociation into two HCO radicals is the most important pathway under atmospheric conditions. The reported wavelength dependence of the quantum yield of the individual channels is based on measurements performed with broad emission lamps and individual measurements determined at selected wavelengths. However, there is still a need to further investigate the exact course of the quantum yield HCO radicals at different pressures.

Acknowledgements

We thank Monserrat Martín Reviejo for her assistance evaluating IR cross-section of glyoxal. This work was carried out with the financial support of the European Union under Contract No. ENV4-CT97-0419 (RADICAL) and MCYT AMB1998-1661-CE. Fundación CEAM is supported by Generalitat Valenciana and BANCAIXA.

References

[1] R. Atkinson, Atmos. Environ. 34 (2000) 2063.
[2] J.G. Calvert, R. Atkinson, K.H. Becker, R.M. Kamens, J.H. Seinfeld, T.J. Wallington, G. Yarwood, The Mechanisms of Atmospheric Oxidation of Aromatic Hydrocarbons, Oxford University Press, Oxford, 2002.
[3] H. Bandow, N. Washida, Bull. Chem. Soc. Jpn. 58 (1985) 2549.
[4] E.C. Tuazon, H. MacLeod, R. Atkinson, W.P.L. Carter, Environ. Sci. Technol. 20 (1986) 383.
[5] R. Volkamer, U. Platt, K. Wirtz, J. Phys. Chem. 105 (2001) 7865.
[6] J.G. Calvert, R. Atkinson, J.A. Kerr, S. Madronich, G.K. Moortgat, T.J. Wallington, G. Yarwood, The Mechanisms of Atmospheric Oxidation of Alkenes, Oxford University Press, Oxford, 2000.
[7] S. Hatakeyama, N. Washida, H. Akimoto, J. Phys. Chem. 90 (1986) 173.
[8] I. Magneron, R. Thevenet, A. Mellouki, G. Le Bras, G.K. Moortgat, K. Wirtz, J. Phys. Chem. A 106 (2002) 2526.
[9] I. Barnes, V. Bastian, K.H. Becker, R. Overath, Z. Tong, Int. J. Chem. Kin. 21 (1989) 499.
[10] G. Yarwood, N. Peng, H. Niki, J. Phys. Chem. 95 (1991) 7330.
[11] I. Magneron, A. Mellouki, G. Le Bras, G.K. Moortgat, A. Horowitz, K. Wirtz, J. Phys. Chem. A 109 (2005) 4552.
[12] A.J. Kean, E. Grosjean, D. Grosjean, R.A. Harley, Environ. Sci. Technol. 35 (2001) 4198.
[13] D. Grosjean, E. Grosjean, A.W. Gertler, Environ. Sci. Technol. 35 (2001) 45.
[14] E. Grosjean, P.G. Green, D. Grosjean, Anal. Chem. 71 (1999) 185.
[15] G.K. Moortgat, D. Grossmann, A. Boddenberg, G. Dallmann, A.P. Ligon, W.V. Turner, S. Gäb, F. Slemr, W. Wieprecht, K. Acker, M. Kibler, S. Schlomski, K. Bächmann, J. Atmos. Chem. 42 (2002) 443.
[16] R. Volkamer, L.T. Molina, M.J. Molina, T. Shirley, W.H. Brune, Geophys. Res. Lett. 32 (2005) L08806, doi:10.1029/2005GL022616.
[17] C.N. Plum, E. Sanhueza, R. Atkinson, W.P.L. Carter, J.N. Pitts Jr., Environ. Sci. Technol. 17 (1983) 479.
[18] G.K. Moortgat, Pure Appl. Chem. 73 (2001) 487.
[19] J.C.D. Brand, Trans. Faraday Soc. 50 (1950) 431.
[20] J.J. Orlando, G.S. Tyndall, Int. J. Chem. Kinet. 33 (2001) 149.
[21] A. Horowitz, R. Meller, G.K. Moortgat, J. Photochem. Photobiol. A Chem. 146 (2001) 19.
[22] R. Volkamer, P. Spietz, J. Burrows, U. Platt, J. Photochem. Photobiol. A Chem. 172 (2005) 35.
[23] J.G. Calvert, J.N. Pitts Jr., Photochemistry, Wiley, New York, 1996.
[24] J.G. Calvert, G.S. Layne, J. Am. Chem. Soc. 75 (1953) 856.
[25] A.O. Langford, C.B. Moore, J. Chem. Phys. 80 (1984) 4211.
[26] L. Zhu, D. Kellis, C.-F. Ding, Chem. Phys. Lett. 257 (1996) 487.
[27] Y. Chen, L. Zhu, J. Phys. Chem. 107 (2003) 4643.
[28] G.K. Moortgat, R.A. Cox, G. Schuster, J.P. Burrows, G.S. Tyndall, J. Chem. Soc. Farad. Trans. II 85 (1989) 809.
[29] J. Tadić, I. Juranić, G.K. Moortgat, J. Photochem. Photobiol. A Chem. 143 (2001) 169.
[30] P. Neeb, O. Horie, G.K. Moortgat, J. Phys. Chem. 102 (1998) 6778.
[31] W.H. Raber, G.K. Moortgat, Progress and Problems in Atmospheric Chemistry, in: J.R. Barker (Ed.), Advanced Series in Physical Chemistry, vol. 3, Word Scientific Publishing Co., Singapore, 1995, pp. 318–373.
[32] The european photoreactor EUPHORE, in: K.H. Becker (Ed.), Final Report of EC Project EV5V-CT92-0059, Wuppertal, Germany, 1996.
[33] R. Atkinson, D.L. Baulch, R.A. Cox, R.F. Hampson Jr., J.A. Kerr, M.J. Rossi, J. Troe, J. Phys. Chem. Ref. Data 26 (1997) 521.
[34] F. Su, J.G. Calvert, J.H. Shaw, J. Phys. Chem. 83 (1989) 3185.
[35] B. Veyret, R. Lesclaux, M.-T. Rayez, J.-C. Rayez, R.A. Cox, G.K. Moortgat, J. Phys. Chem. 93 (1989) 2368.
[36] J.P. Burrows, G.K. Moortgat, G.S. Tyndall, R.A. Cox, M.E. Jenkin, G.D. Hayman, B. Veyret, J. Phys. Chem. 93 (1989) 2375.
[37] D.M. Koch, N.H. Khieu, G.H. Peslherbe, J. Phys. Chem. A 105 (2001) 3598.
[38] L.M. Dobeck, H.M. Lambert, W. Kong, P.J. Pisano, P.L. Houston, J. Phys. Chem. A 103 (1999) 10312.
[39] C. Chang, I.-C. Chen, J. Chem. Phys. 116 (2002) 2447.
[40] S. Koch, G.K. Moortgat, J. Phys. Chem. A 102 (1998) 9142.
[41] G.K. Moortgat (Ed.), RADICAL: Evaluation of Radical Sources in Atmospheric Chemistry Through Chamber and Laboratory Studies, ENV4-CT97-0419, JRC, Ispra, Italy, EUR 20254 EN, 2002, for copies: moo@mpch-mainz.mpg.de.